Computer simulation of tension experiments of a thin film using an atomic model

Yeau-Ren Jeng and Chung-Ming Tan
Department of Mechanical Engineering, National Chung Cheng University, Chia-Yi, Taiwan
(Received 24 September 2001; published 23 April 2002)

The stress and strain induced in a very thin film under uniaxial tension are analyzed by an atomic-scale model approach that is based on the nonlinear finite element formulation. Certain aspects of the dependence of material properties on their size are addressed. This method is quasistatic, thereby greatly reducing required computation time. The numerical results show that the tension varies nonlinearly with the elongation and the stiffness of the thin film decreases with the decrease of the thickness. Evidence reveals that the variation of the distribution of the stress near the free surfaces is one of the causes of the decrease in the stiffness of the thin film.

DOI: 10.1103/PhysRevB.65.174107 PACS number(s): 81.40.Jj

I. INTRODUCTION

The manufacturing and application techniques of thin films are being widely used in various fields, such as sensors and actuators, semiconductor, and tribology.[1–3] The thin film is such an important basic element for advanced functional materials and devices that knowledge concerning its mechanical properties becomes more and more important. The values of physical quantities, such as the coefficient of elasticity and thermal expansion obtained from the bulk material are used for the thin film because of experimental difficulties.

The most fundamental mechanical properties of the thin film, which are defined on the precepts of continuum mechanics, are assumed to be independent of size. However, with a nanoscale dimension, that the properties of a material depend on the size of the system is commonly expected and observed.[4] Obviously, the physical properties of the bulk cannot be applied to the thin film with the nanometer dimension in the thickness. Furthermore, the nature of this size dependence will further depend on the material in question.

The atomic-scale simulation of the solid argon thin film under uniaxial tension was carried out by Iwaki, who calculated the stress and strain induced in the film under tension by means of two-dimensional molecular-dynamics (MD) simulation, and found that more than 130 particles are necessary in the region for the stress concept to be applicable in continuum mechanics.[5] Mehrez and Ciraci had investigated the yielding and fracture mechanisms of copper nanowires, which are pulled by an external agent using MD simulation.[6] Their study clarified that the yielding and fracture mechanisms depend on the size, atomic arrangement, and temperature. Miller and Shenoy proposed a simple theoretical model that may predict the size dependence of effective stiffness properties of nanosized structural elements.[7] Miller and Shenoy investigated the size dependence of elastic properties by virtue of evaluating the surface modulus, which is different from that of the bulk. Thus, effective stiffness properties of nanosized structural elements are studied quantitatively. Basically, that was still a macroscopic analytical method.

From the relevant researches mentioned above, it is clear that the MD simulation is the main simulation method from the molecular point of view. Molecular dynamics has wide applicability such that it can simulate, in principle, at least, the phenomena at a molecular level, including diffusion, motion of dislocation, and fracture.[8–16] However, it requires extensive computing time. For example, if a physical phenomenon is to be simulated for 1 sec by 10^{-15} time resolution, computation for 10^{15} time increments is needed for each atom. It is a high computational cost even for a supercomputer.

In this work, instead of MD simulation, we adopt an alternative approach. Based on the fact that in condensed systems, atoms or molecules always oscillate around the minimum-energy positions. We are to follow the changes of the minimum-energy positions that are the mean positions of each oscillating atom. The computation in this way is quasistatic, thereby greatly reducing the computing time. The objective of this study is to clarify that how the stress and strain distribute in the thin film qualitatively. We utilized the finite element method with atomic model to study the size dependence of elastic properties.

II. COMPUTER SIMULATION

A. The thin-film model

The thin-film configuration consisting of particles of copper atoms is shown in Fig. 1(a). This is a two-dimensional model. The arrangement of atoms can be viewed as one of the family of close-packed planes, {111}, in a face-centered cubic monocrystalline copper. The x axis is taken to point to one of the family of close-packed directions, $\langle 110 \rangle$. It is in the direction of the thickness. The tension loads along the y axis, i.e., the direction of the length. In Fig. 1(b), the profile of the thin film could be considered to lie in the oblique plane shown in the three-dimensional sketch of the copper crystal. Unlike the MD simulation, the periodic boundary condition cannot be employed to simulate the infinite domain condition. Therefore, the boundary conditions in the lower end of the length are that the atoms are fixed in the y axis direction but free to move in the x direction, and in the upper end the atoms are under the constraint that the displacements of each of the atoms in the y axis direction are the same.

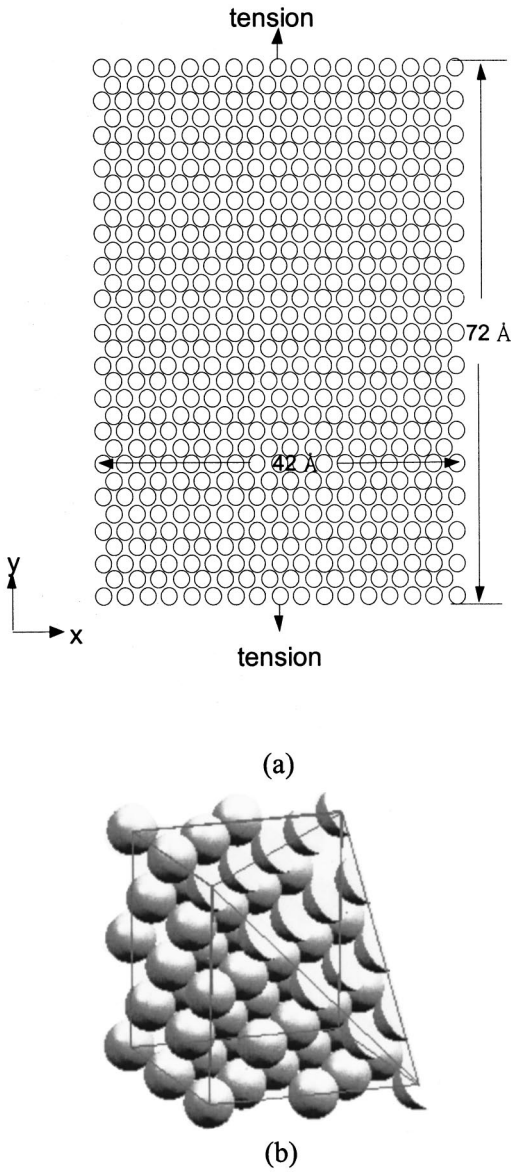

FIG. 1. The atomic model of the thin film.

The interatomic potential energy is assumed to be described as the sum of the pairwise empirical potentials that depend only on the distance of the atoms. ''Morse'' potential is employed to be the pairwise potential in this study. It has the following form:

$$\phi(r_{ij}) = D\{\exp[-2\alpha(r_{ij}-r_0)] - 2\exp[-\alpha(r_{ij}-r_0)]\}, \tag{1}$$

where r_{ij} is the distance between atoms ''i'' and ''j,'' and D, α, and r_0 are constants to be determined based on the physical properties of the corresponding material. This potential produces a repulsive force in a short range, attractive force in a medium range, and decays smoothly to zero in a long range, as shown in Fig. 2. The appropriate constant values for copper metal are given in Fig. 2.[17]

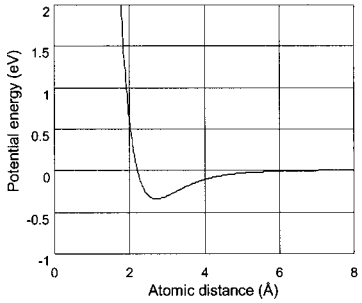

	Cu - Cu
D	0.3429
α	1.3588
r_o	2.7202

FIG. 2. Potential energy curve used in the experiment.

B. The method of simulation

The process of the tension experiment is simulated by increasing the displacements of the atoms in the upper end of the thin film. During the process, the copper atoms in the film always move to the minimum-energy positions under the equilibrium condition. Thus, we establish a computationally more efficient procedure in the following, based on the nonlinear finite element formulation.[17] As shown in Fig. 3, the arbitrary two atoms ''i'' and ''j'' are regarded as two nodes, and their potential as one element. Assume that the atom ''i'' is located at the position (x_i, y_i) with displacement u_i, v_i in the x,y directions, respectively. Then by defining the nodal displacement vector $\{\mathbf{u}\}_{ij}$ and the corresponding nodal force vector $\{\mathbf{F}\}_{ij} = (f_i, g_i, f_j, g_j)^T$ for the i and j atoms, the total pair potential energy is formulated as

$$E_{ij} = \phi(r_{ij}) - \{\mathbf{u}\}_{ij}^T \{\mathbf{F}\}_{ij} \tag{2}$$

where the superscript ''T'' means transpose, while the atomic distance r_{ij} is given by

$$r_{ij} = \{(x_i + u_i - x_j - u_j)^2 + (y_i + \nu_i - y_j - \nu_j)^2\}^{1/2} \tag{3}$$

so that its differential with respect to $\{\mathbf{u}\}_{ij}$ is

$$d\mathbf{r}_{ij} = [x_i + u_i - x_j - u_j, y_i + \nu_i - y_j - \nu_j, -(x_i + u_i - x_j - u_j), -(y_i + \nu_i - y_j - \nu_j)]d\{\mathbf{u}\}_{ij} = [B]d\{\mathbf{u}\}_{ij}. \tag{4}$$

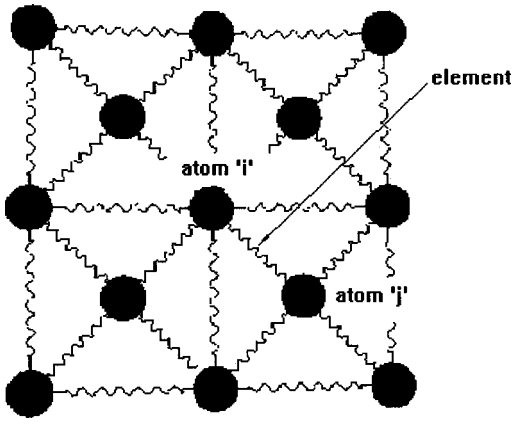

FIG. 3. Finite element model on atomic scale.

Then the principle of minimum work enforces the minimization of $\mathbf{E}_{ij}$ with respect to $\{\mathbf{u}\}_{ij}$ such that

$$\frac{\partial \mathbf{E}_{ij}}{\partial \{\mathbf{u}\}_{ij}} = \left(\frac{\partial \phi}{\partial r_{ij}}\right)[B]^T - \{\mathbf{F}\}_{ij} = \{0\}. \tag{5}$$

Equation (5) is the element equilibrium equation that represents the equilibrium of forces acting on the atoms i and j. Then we define a residual force $\{\boldsymbol{\xi}\}_{ij}$ by

$$\{\boldsymbol{\xi}\}_{ij} = \left(\frac{\partial \phi}{\partial \mathbf{r}_{ij}}\right)[B]^T - \{\mathbf{F}\}_{ij}. \tag{6}$$

And when the equilibrium equation is achieved by iteration procedure, it would converge to zero with an acceptable tolerance. In order to solve the nonlinear equilibrium equation by iteration procedure, we differentiate $\{\boldsymbol{\xi}\}_{ij}$ with respect to $\{\mathbf{u}\}_{ij}$

$$\begin{aligned} d\{\boldsymbol{\xi}\}_{ij} &= d\left(\frac{\partial \phi}{\partial \mathbf{r}_{ij}}\right)[B]^T + \left(\frac{\partial \phi}{\partial \mathbf{r}_{ij}}\right) d[B]^T \\ &= [B]^T \left(\frac{\partial^2 \phi}{\partial \mathbf{r}_{ij}^2}\right) d\mathbf{r}_{ij} + \left(\frac{\partial \phi}{\partial \mathbf{r}_{ij}}\right) d[B]^T \\ &= ([K]_{ij} + [K_\sigma]_{ij}) d\{\mathbf{u}\}_{ij} \\ &= [K_T]_{ij} d\{\mathbf{u}\}_{ij}, \end{aligned} \tag{7}$$

where

$$[K]_{ij} = [B]^T \left(\frac{\partial^2 \phi}{\partial r_{ij}^2}\right)[B] \tag{8}$$

and

$$[K_\sigma]_{ij} = \left(\frac{\phi}{\mathbf{r}_{ij}}\right)\left[\frac{\partial [B]^T}{\partial u_i}, \frac{\partial [B]^T}{\partial \nu_i}, \frac{\partial [B]^T}{\partial u_j}, \frac{\partial [B]^T}{\partial u_j}\right]. \tag{9}$$

Equation (8) can be obtained by substituting Eq. (4) for the $d\mathbf{r}_{ij}$ in Eq. (7). Then according to the usual assembly procedure of the finite element formulation, element Eq. (7) is assembled to obtain the total system equation

$$d\{\boldsymbol{\xi}\} = [K_T] d\{\mathbf{u}\}. \tag{10}$$

Similarly, Eq. (5) is assembled to obtain the equilibrium equation of the total system

$$\sum_{i \neq j} \left(\frac{\partial \phi}{\partial \mathbf{r}_{ij}}\right)[B]^T - \{\mathbf{F}\}_{ij} = \{\mathbf{f}\}_{\text{internal}} \{\mathbf{F}\}_{\text{external}} = \{0\}. \tag{11}$$

In terms of finite element formulation, Eq. (10) is the tangent stiffness equation, and $\{\mathbf{f}\}_{\text{internal}}$ and $\{\mathbf{F}\}_{\text{external}}$ in Eq. (11) are the internal force vector and the external force vector, respectively. Before proceeding to solve the nonlinear equilibrium Eq. (5) by iteration procedure, we would like to explain how the boundary conditions and the constraints are achieved.[18] The tangent stiffness equation can be assumed to be of the form

$$d\{\boldsymbol{\xi}\} = \begin{pmatrix} d\xi_f \\ d\xi_p \end{pmatrix} = [K_T] d\{\mathbf{u}\} = \begin{bmatrix} K_{ff} & K_{fp} \\ K_{pf} & K_{pp} \end{bmatrix} \begin{pmatrix} du_f \\ du_p \end{pmatrix}. \tag{12}$$

In this study, the prescribed boundary conditions are that the components of du_p are constrained to zero, and this is achieved by altering Eq. (12) to become

$$d\{\boldsymbol{\xi}\} = \begin{pmatrix} d\xi_f \\ 0 \end{pmatrix} = [K_T] d\{\mathbf{u}\} = \begin{bmatrix} K_{ff} & 0 \\ 0 & I \end{bmatrix} \begin{pmatrix} du_f \\ 0 \end{pmatrix}. \tag{13}$$

In addition, the satisfaction of the constraints is written in the form

$$[C] d\{\mathbf{u}\} = \{0\}. \tag{14}$$

We modify the tangent stiffness matrix $[K_T]$ by adding a penalty matrix $[C]^T \alpha [C]$, then the tangent stiffness equation becomes

$$d\{\boldsymbol{\xi}\} = ([K_T] + [C]^T \alpha [C]) d\{\mathbf{u}\} \tag{15}$$

where α is a very large number compared with any element of the matrix $[K_T]$. After imposing the boundary conditions and constraints, we adopt the Newton-Raphson iterative technique to solve the equilibrium Eq. (11) using a suitable displacement control scheme in the following. Assume that the external force vector $\{\mathbf{F}\}$ keeps a specified form during the process of iteration

$$\{\mathbf{F}\}^i = \{\mathbf{F}\}^{i-1} + \lambda^i \{\hat{F}\}, \quad i = 1,2, \ldots, \tag{16}$$

where $\{\hat{F}\}$ is the reference load vector. Substituting Eq. (16) into Eq. (10), the iterative tangent stiffness equation become

$$[K_T] d\{\mathbf{u}\}^i = \lambda^i \{\hat{F}\} + d\{\boldsymbol{\xi}\}^i, \quad i = 1,2, \ldots . \tag{17}$$

Consequently, the iterative displacement increment can be written in a similar form

$$d\{u\}^i = \lambda^I \{u\}_a^i + d\{u\}_b^i, \quad i = 1,2, \ldots \tag{18}$$

where for $i = 1,2, \ldots,$

$$\begin{aligned} [K_T]\{\mathbf{u}\}_a^i &= \{\hat{F}\}, \\ [K_T] d\{\mathbf{u}\}_b^i &= d\{\boldsymbol{\xi}\}^i. \end{aligned} \tag{19}$$

The ''displacement'' control scheme means that we keep the qth component of the increment displacement vector constant during the process of iteration as follows:

$$\begin{aligned} \lambda^i \mathbf{u}_{aq}^i + d\mathbf{u}_{bq}^i &= d\mathbf{u}_q^i \\ d\mathbf{u}_q^i &= \begin{cases} d\mathbf{u}_q, & i = 1 \\ 0, & i > 1 \end{cases}. \end{aligned} \tag{20}$$

By the iterative solution strategy mentioned above, we can obtain the whole equilibrium path of the tension experiment.

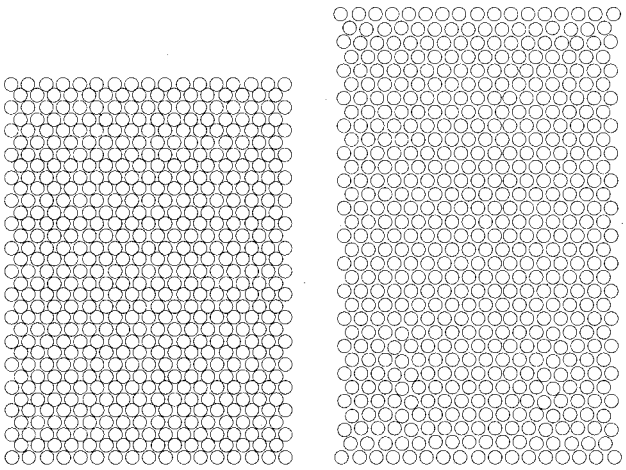

FIG. 4. The arrangement of the atoms before and after deformation.

III. RESULTS AND DISCUSSION

A. Tension vs deformation relation

A typical particle representation of the thin film after the deformation observed in the simulation is shown in Fig. 4. In the figure, except at both ends in the longitudinal direction, there is no change in the arrangement of the atoms. This implies that no dislocation or slip has occurred at this high strained level. The finite length effect will be examined in the following section. To illustrate the effect of the nanometer dimension in the thickness of the film and the efficiency of the finite element approach on atomic scale, the tension vs elongation curves of three different thicknesses are shown in Fig. 5. Usually, the tension experiment proceeds at the quasistatic condition. This is unavailable in the MD simulation in the literature.[6] Owing to the high time resolution required in MD simulation, the stretching velocity ranges from 0.4–0.5 m/sec. Since the approach established in this study is quasistatic, our simulation need not consider the stretching velocity. The computing time to obtain the variation of elongation with tension is about 8 min on a personal computer with a 1.2 G AMD CPU, which is about two orders of magnitude less in computing time compared with the MD simulation. As shown in Fig. 5, the applied external force increases nonlinearly with the increase in elongation. The nonlinearity can be attributed to the pairwise potentials of the atoms. The arrangement of particles, as shown in the Fig. 4, is unaltered until the applied force becomes maximum. After that the arrangement of particles is disordered because the structure is unstable.[19] Consequently, the iteration process from Eq. (16) to Eq. (20) diverges as soon as the structure is unstable. In addition, the effect of the decrease in the thickness is obvious from the curves in the Fig. 5. The stiffness of the thin film decreases with the decrease of the thickness. The reasons of this phenomenon will be clear after the investigation of the stress and strain distribution in the cross section of the thickness.

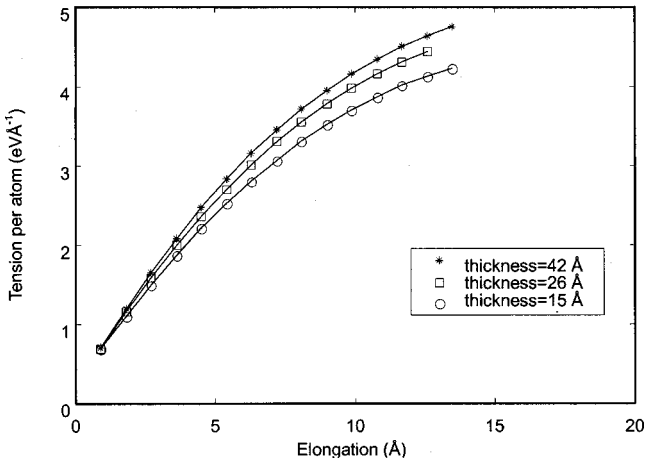

FIG. 5. Tension vs elongation curves of the thin film.

B. Stress/strain analysis

A general idea to derive values of continuum mechanics from those of an atomic model should be mentioned. Although the displacement in the atomic model can be defined only at the points of each atom, the displacement in the continuum model exists even at a point between two atoms. This implies that the displacement at one point in the continuum model should be defined as a kind of interpolation of those of the surrounding atoms. In this study, we generalize this idea such that the displacement at a point in the continuum model is the weighted average of the values of the surrounding atoms.[20] Thus, the displacement $\overline{u}(\mathbf{r}_p)$ at the point $\mathbf{r}_p=(x_p,y_p)$ in the continuum model is defined by

$$\overline{u}(r_p)=\sum_q w(\mathbf{r}_p,\mathbf{r}_q)u(r_q) \tag{21}$$

where $\mathbf{r}_p=(x_p,y_p)$ and $\mathbf{u}(\mathbf{r}_q)$ are the position and displacement of the atom q in the atomic model, and $w(r_p,r_q)$ is the weight function which should satisfy

$$\sum_q w(\mathbf{r}_p,\mathbf{r}_q)=1,$$

$$w(\mathbf{r}_p,\mathbf{r}_q)=w(\mathbf{r}_q,\mathbf{r}_p). \tag{22}$$

The weight function used here is

$$w(\mathbf{r}_p,\mathbf{r}_q)=C_{pq}\exp\left[-\frac{|\mathbf{r}_p-\mathbf{r}_q|^2}{2\sigma^2}\right], \tag{23}$$

where the constant C_{pq} is so chosen as to satisfy condition (22), and the constant σ determines the range of averaging.

The strain at point $\mathbf{r}_p$ can be defined in the usual manner. By redefining the x and y components of the displacement of atom q by $u(r_q)$ and $v(r_q)$, respectively, the three components of strain are given by

$$\overline{\varepsilon_x}(\mathbf{r}_p)=\frac{\partial}{\partial x_p}\sum_q w(\mathbf{r}_p,\mathbf{r}_q)u(\mathbf{r}_q), \tag{24}$$

$$\overline{\varepsilon_y}(\mathbf{r}_p)=\frac{\partial}{\partial y_p}\sum_q w(\mathbf{r}_p,\mathbf{r}_q)v(\mathbf{r}_q), \tag{25}$$

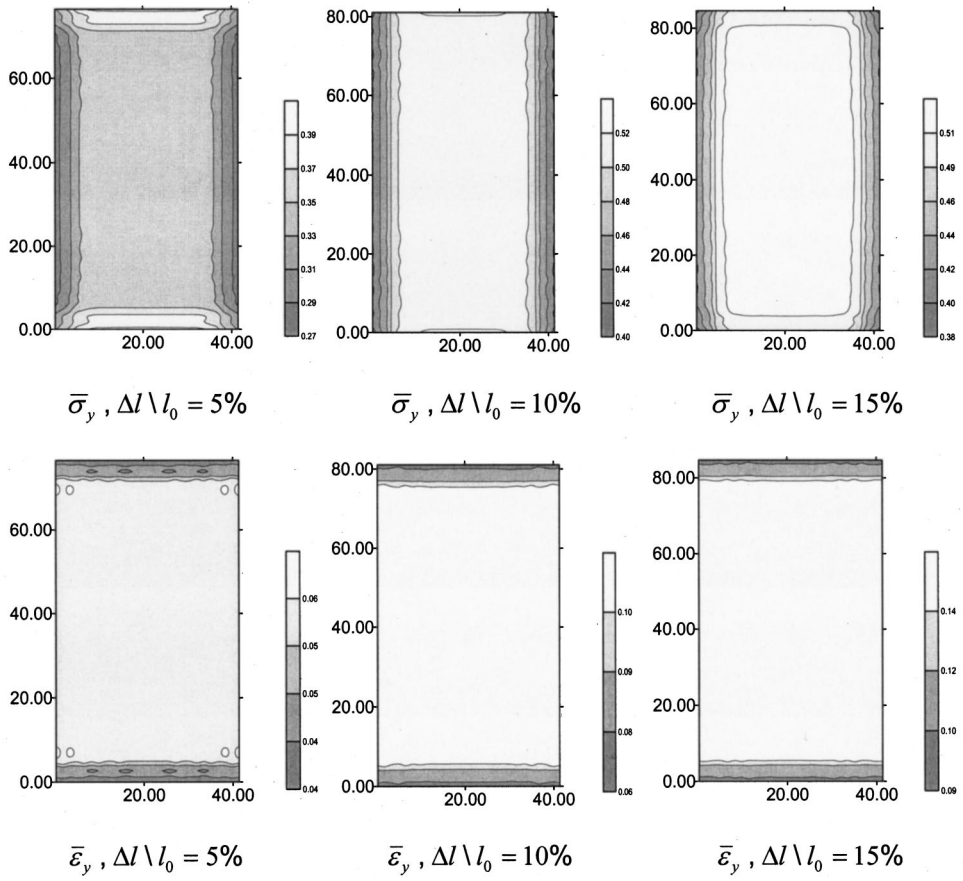

FIG. 6. The variations of the distributions of the stress and strain during the process of stretching.

$$\overline{\gamma}_{xy}(\mathbf{r}_p) = \frac{\partial}{\partial x_p} \sum_q w(\mathbf{r}_p, \mathbf{r}_q) u(\mathbf{r}_q) + \frac{\partial}{\partial y_p} \sum_q w(\mathbf{r}_p, \mathbf{r}_q) \nu(\mathbf{r}_q). \tag{26}$$

The stress at point $\mathbf{r}_p$ is defined in a similar way as the displacement is. First, we measure the stress at atom q by summing all the forces passing through the planar faces of the computational box at which atom q is centered according to the following equations:[21]

$$\sigma_x(\mathbf{r}_q) = \frac{1}{A} \sum_{q<s} \frac{F(\mathbf{r}_{qs})}{\mathbf{r}_{qs}} (\Delta x)^2, \tag{27}$$

$$\sigma_y(\mathbf{r}_q) = \frac{1}{A} \sum_{q<s} \frac{F(\mathbf{r}_{qs})}{\mathbf{r}_{qs}} (\Delta y)^2, \tag{28}$$

$$\tau_{xy}(\mathbf{r}_q) = \frac{1}{A} \sum_{q<s} \frac{F(\mathbf{r}_{qs})}{\mathbf{r}_{qs}} (\Delta x \cdot \Delta y), \tag{29}$$

where A is the area of the side of the cubic computational box, $\mathbf{r}_{qs}$ is the distance between atom q and s, $\mathbf{F}(\mathbf{r}_{qs})$ is the force between atoms q and s.

Then the stress components $\overline{\sigma}_x$, $\overline{\sigma}_y$, and $\overline{\tau}_{xy}$ in the continuum model are defined in the weighted mean manner such that

$$\overline{\sigma}_x(\mathbf{r}_p) = \sum_q w(\mathbf{r}_p, \mathbf{r}_q) \sigma_x(\mathbf{r}_q), \tag{30}$$

$$\overline{\sigma}_y(\mathbf{r}_p) = \sum_q w(\mathbf{r}_p, \mathbf{r}_q) \sigma_y(\mathbf{r}_q), \tag{31}$$

$$\overline{\tau}_{xy}(\mathbf{r}_p) = \sum_q w(\mathbf{r}_p, \mathbf{r}_q) \tau_{xy}(\mathbf{r}_q). \tag{32}$$

The equations described above have been applied to the results of the nanoscale tension experiment simulation as follows. First, we examine the distribution of stress and strain induced in the thin film during the process of the tension experiment. Figure 6 shows the variations of the distribution of the stress and strain components in the loading direction, at three different stretched levels. The distribution of the strain component $\overline{\varepsilon}_y$ does not have any abrupt change, whereas the distribution of the stress component $\overline{\sigma}_y$ has obvious changes. The stress component $\overline{\sigma}_y$ near the free surfaces decreases during the process of pulling. In contrast, the strain component $\overline{\varepsilon}_y$ does not decrease at the free surfaces, but does decrease at both the ends. Hence, we need further examination of the effects of the free surfaces and the finite length.

We took the thickness and length of the thin film as two parameters to investigate how they influence the distributions of the stress component $\overline{\sigma}_y$ and the strain component $\overline{\varepsilon}_y$ qualitatively. Therefore, the reason why the stiffness of the thin film decreases with the decrease of its thickness will be illustrated. Figure 7 shows how the distribution of the stress component $\overline{\sigma}_y$ changes with variations of the two parameters

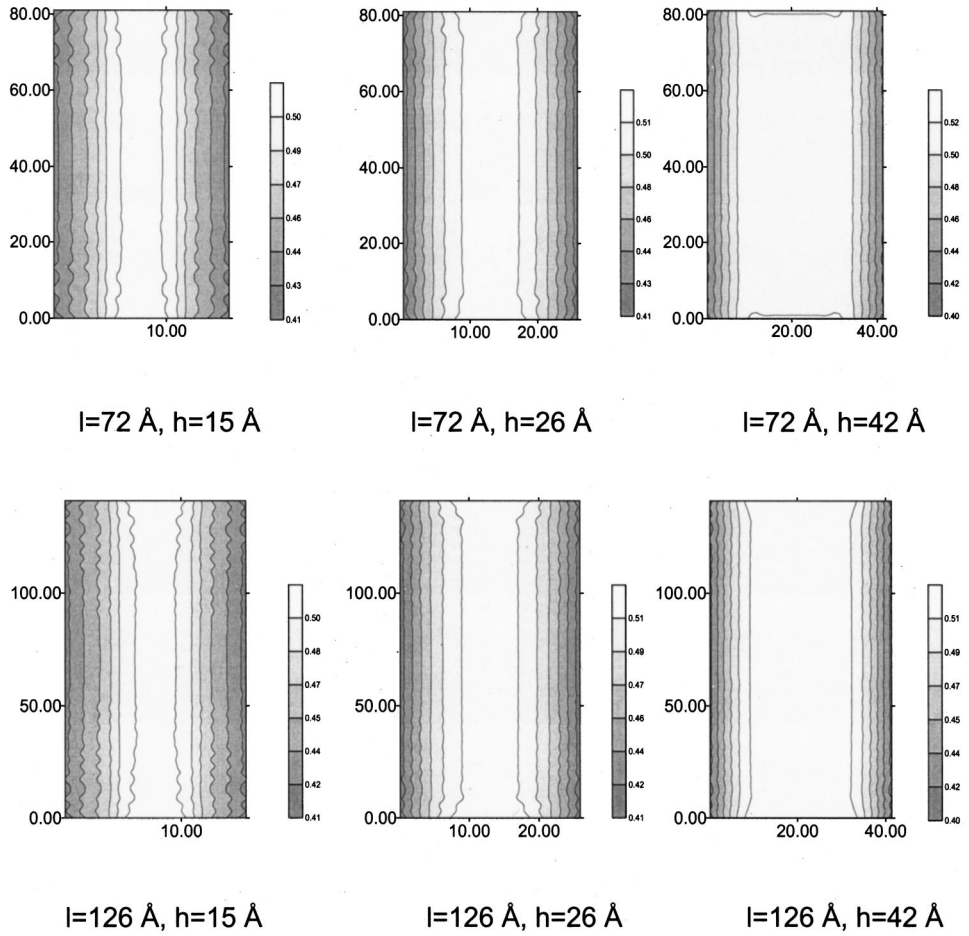

FIG. 7. The influence of length and thickness on the distribution of the stress field.

at the same stretched level. In this figure, the three columns represent the distributions of three different thicknesses, and the two subplots in each column represent the distributions of two different lengths with the same thickness. The six subplots in the figure are so scaled as to be of the same size for the convenience of comparison. Comparing the two subplots in each column, we find that the magnitude of the finite length has little influence on the distribution of the stress component $\overline{\sigma_y}$. In contrast, comparing the three columns, it is found that the range of the region adjacent to the free surfaces in which the stress decreases gradually becomes larger with the decrease of the thin-film thickness. Figure 8 shows the influence of the two parameters on the distribution of the strain component $\overline{\varepsilon_y}$. The six subplots are arranged and scaled in the same manner as those in Fig. 7. It is clear that at both the free surfaces of the thin film these two parameters have no influence on the distribution of the strain component $\overline{\varepsilon_y}$. However, from the six subplots, we see that the strain component $\overline{\varepsilon_y}$ decreases gradually at the both ends of the length. Figure 8 also depicts that the affected area is of about the same size. Therefore, due to the scaling, the ranges of the region where the strain component $\overline{\varepsilon_y}$ decrease in the lower three subplots look larger than those in the upper three subplots. From the discussion above, we conclude that the range of the region adjacent to the free surfaces of the thin film, where the stiffness of the material decreases, becomes larger as the thickness of the thin film decreases. Therefore, the reason for the phenomenon that the stiffness decreases with decrease in thickness can be clarified. In addition, the influence of the ends of finite length is limited in a specific distance adjacent to the boundaries. This phenomenon is similar to Saint-Venant's principle in solid mechanics.

By means of the stress and strain analysis presented above, we have clarified the mechanism of the degradation of the stiffness of the thin film as its thickness decreases. This point of view is different from that of the relevant research by Miller and Shenoy.[7] They only account for the effect of free surfaces at the skin. In this study, we provide a microscopic viewpoint. Furthermore, we have investigated further the effect of the region adjacent to free surfaces.

IV. CONCLUSION

In this work, two arbitrary atoms are considered as two nodes, their potential as one element. Thus, we formulate the atomic thin-film model in the manner that is analogous with the nonlinear finite element method. The displacement control strategy is adopted to solve the static equilibrium equations. The stress and strain defined in the continuum mechanics are derived from the weighted average of those in the atomic model. Taking the length and thickness as two parameters, the distributions of the stress and strain fields induced in the thin film under uniaxial tension are studied. From our investigation, the following conclusions can be reached.

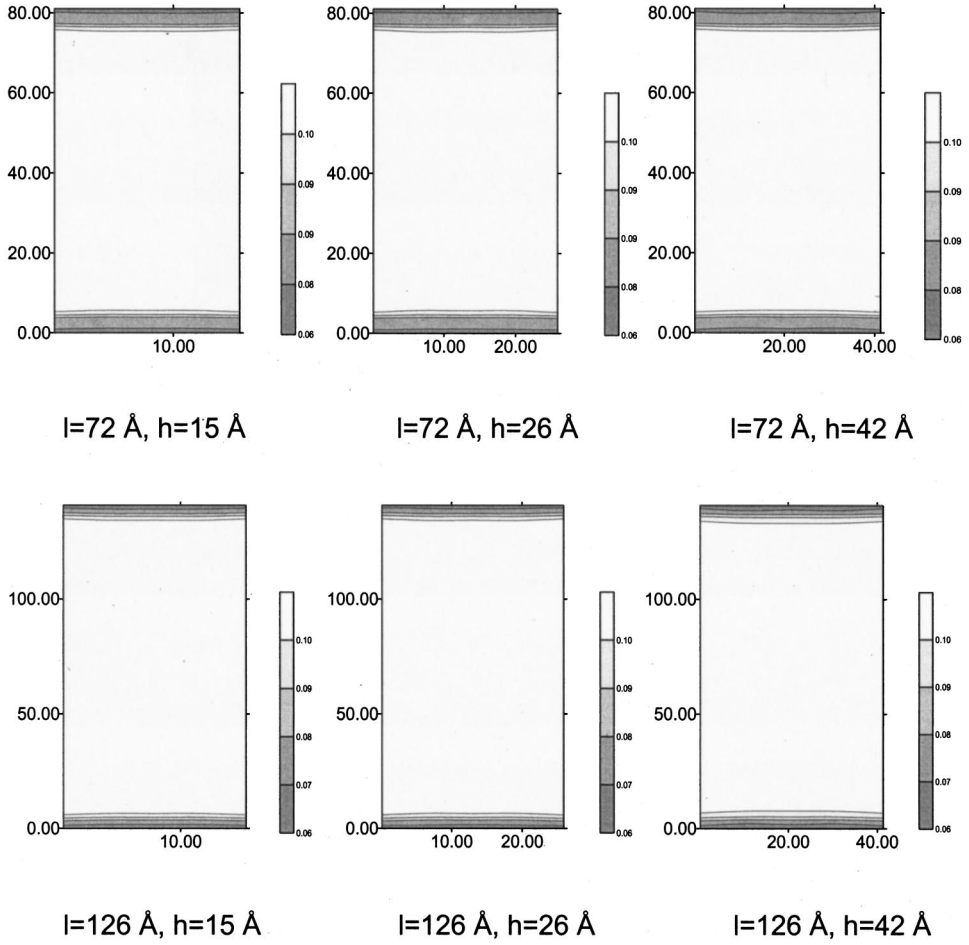

FIG. 8. The influence of length and thickness on the distribution of the strain field.

(1) Our study shows that the current approach is more efficient than the conventional MD simulation.

(2) The tension-elongation curves obtained from the simulation show that the tension increases nonlinearly with increase in elongation. The nonlinearity depends on the particle potential.

(3) The tension experiment shows that the stiffness of the thin film decreases with the decrease of its thickness.

(4) From the stress and strain analysis, it is found that the decrease in the stress in the regions adjacent to the free surfaces is one of the causes of the decrease in the stiffness as the thin-film thickness decreases.

[1] W. R. Ashurst, C. Yau, C. Carraro, C. Lee, G. J. Kluth, R. T. Howr, and R. Maboudian, Sens. Actuators A **91**, 239 (2001).
[2] A. K. Jamting, J. M. Bell, M. V. Swain, and N. Schwarzer, Thin Solid Films **308-309**, 304 (1997).
[3] S. P. Baker, Thin Solid Films **308-309**, 289 (1997).
[4] U. Landman, Solid State Commun. **107**, 693 (1998).
[5] T. Iwaki, JSME Int. J., Ser. A **39**, 346 (1996).
[6] H. Mehrez and S. Ciraci, Phys. Rev. B **56**, 12 632 (1997).
[7] R. E. Miller and V. B. Shenoy, Nanotechnology **11**, 139 (2000).
[8] M. Doyama, Nucl. Instrum. Methods **102**, 107 (1995).
[9] I. I. Gainutdinov, Y. T. Pavlukhin, and V. V. Boldyrev, J. Alloys Compd. **234**, 101 (1996).
[10] M. Doyama, Nanostruct. Mater. **9**, 689 (1997).
[11] T. A. Michalske and J. E. Houston, Acta Mater. **46**, 391 (1998).
[12] M. Doyama, T. Nozake, Y. Kogure, and T. Yokotsuka, Nanostruct. Mater. **12**, 333 (1999).
[13] P. Heino and E. Ristolainen, Nanostruct. Mater. **11**, 587 (1999).
[14] F. F. Abraham, D. Brodbeck, W. E. Rudge, and X. Xu, J. Mech. Phys. Solids **45**, 1595 (1997).
[15] Q. H. Tang and T. C. Wang, Acta Mater. **46**, 5313 (1998).
[16] T. Nozaki, M. Doyama, Y. Kogure, and T. Yokotsuka, Thin Solid Films **334**, 221 (1998).
[17] T. Inamura, H. Suzuki, and N. Takezawa, Int. J. Jpn. Soc. Precis. Eng. **25**, (1991).
[18] M. A. Crisfield, *Non-linear Finite Element Analysis of Solids and Structures*, (Wiley, New York, 1997).
[19] S. Yip, M. Tang, J. Li, and J. Wang, Mater. Sci. Eng., A **317**, 236 (2001).
[20] T. Inamura, N. Takezawa, and Y. Kumaki, CIRP Ann. **42**, 79 (1993).
[21] W. Sekkal, H. Aourag, and M. Certier, Comput. Mater. Sci. **9**, 295 (1998).